Supplementary Material

Translational Two-Pore PBPK Model to Characterize Whole-Body Disposition of Different-Size Endogenous and Exogenous Proteins

Shufang Liu[1,*], Yingyi Li[1], Zhe Li[1], Shengjia Wu[1], John M. Harrold[2], Dhaval K. Shah[1,*]

[1] Department of Pharmaceutical Sciences, School of Pharmacy and Pharmaceutical Sciences, The State University of New York at Buffalo, Buffalo, NY

[2] Pharmacometrics & Systems Pharmacology, Pfizer Inc, South San Francisco, California, USA

[*]**Co-Corresponding authors:**

Dhaval K. Shah, PhD
Department of Pharmaceutical Sciences
455 Pharmacy Building, School of Pharmacy and Pharmaceutical Sciences
University at Buffalo, The State University of New York
Buffalo, New York 14214-8033
Telephone: 716-645-4819
E-mail: dshah4@buffalo.edu

Shufang Liu
Department of Pharmaceutical Sciences
457 Pharmacy Building, School of Pharmacy and Pharmaceutical Sciences
University at Buffalo, The State University of New York
Buffalo, New York 14214-8033
E-mail: shufangl@buffalo.edu

Steady state determination in the PBPK model

To facilitate the model development and the estimation process, we applied the methodology developed by Abuqayyas and Harrold [1].

For endogenous IgG,

$$\Delta_{SS}^{IgG} = \begin{cases} C\_0_{Plasma}^{enIgG} - C_{Plasma}^{enIgG}, & time < t_{SS} \\ 0, & time \geq t_{SS} \end{cases} \quad (1)$$

$$Ksyn_{enIgG} = \begin{cases} 0, & \mu_I \cdot AUC\Delta_{SS}^{IgG} < 0 \\ \mu_I \cdot AUC\Delta_{SS}^{IgG}, & \mu_I \cdot AUC\Delta_{SS}^{IgG} \geq 0 \end{cases} \quad (2)$$

Where Δ_{SS}^{IgG} is the difference between the known steady-state IgG concentration ($C\_0_{Plasma}^{enIgG}$) and simulated real-time IgG concentration in plasma (C_{Plasma}^{enIgG}), and t_{SS} is the time point at which the steady state has been reached. The synthesis rate of endogenous IgG ($Ksyn_{enIgG}$) serves as a secondary parameter. $AUC\Delta_{SS}^{IgG}$ is the cumulative area under the curve (AUC) of Δ_{SS}^{IgG} at a given point in time, and μ_I is an integral controller tuning parameter that controls the speed of stabilization.

This process is shown graphically in Supplementary Figure 1. Initially, $Ksyn_{enIgG}$ is 0, and thus C_{Plasma}^{enIgG} becomes lower than $C\_0_{Plasma}^{enIgG}$, so that $AUC\Delta_{SS}^{IgG}$ increases (the green region), leading to increased $Ksyn_{enIgG}$. As $Ksyn_{enIgG}$ keeps increasing, C_{Plasma}^{enIgG} will exceed $C\_0_{Plasma}^{enIgG}$ at some point. This will lead to Δ_{SS}^{IgG} becoming negative (orange region), causing $AUC\Delta_{SS}^{IgG}$ to decrease, and a proportional (μ_I) decrease in $Ksyn_{enIgG}$. This process continues until C_{Plasma}^{enIgG} stabilizes at $C\_0_{Plasma}^{enIgG}$ at t_{SS}, after which $Ksyn_{enIgG}$ is fixed to its value at t_{SS}. In the model, t_{SS} is set as the time of drug administration (i.e., 0), and the simulation begins at -500 hours, so that there is enough stabilization time.

The steady state of endogenous albumin is defined in a similar manner.

$$\Delta_{SS}^{Alb} = \begin{cases} C\_0_{Plasma}^{enAlb} - C_{Plasma}^{enAlb}, & time < t_{SS} \\ 0, & time \geq t_{SS} \end{cases} \quad (3)$$

$$Ksyn_{enAlb} = \begin{cases} 0, & \mu_I \cdot AUC\Delta_{SS}^{Alb} < 0 \\ \mu_I \cdot AUC\Delta_{SS}^{Alb}, & \mu_I \cdot AUC\Delta_{SS}^{Alb} \geq 0 \end{cases} \quad (4)$$

Note that μ_I is assigned the value of 1/h in the current model, but the optimal range of μ_I can be different by orders of magnitude in another system (or when the parameter units change). Therefore, it is vital to check if steady states have been reached at t_{SS} by adjusting μ_I values (Supplementary Figure 2).

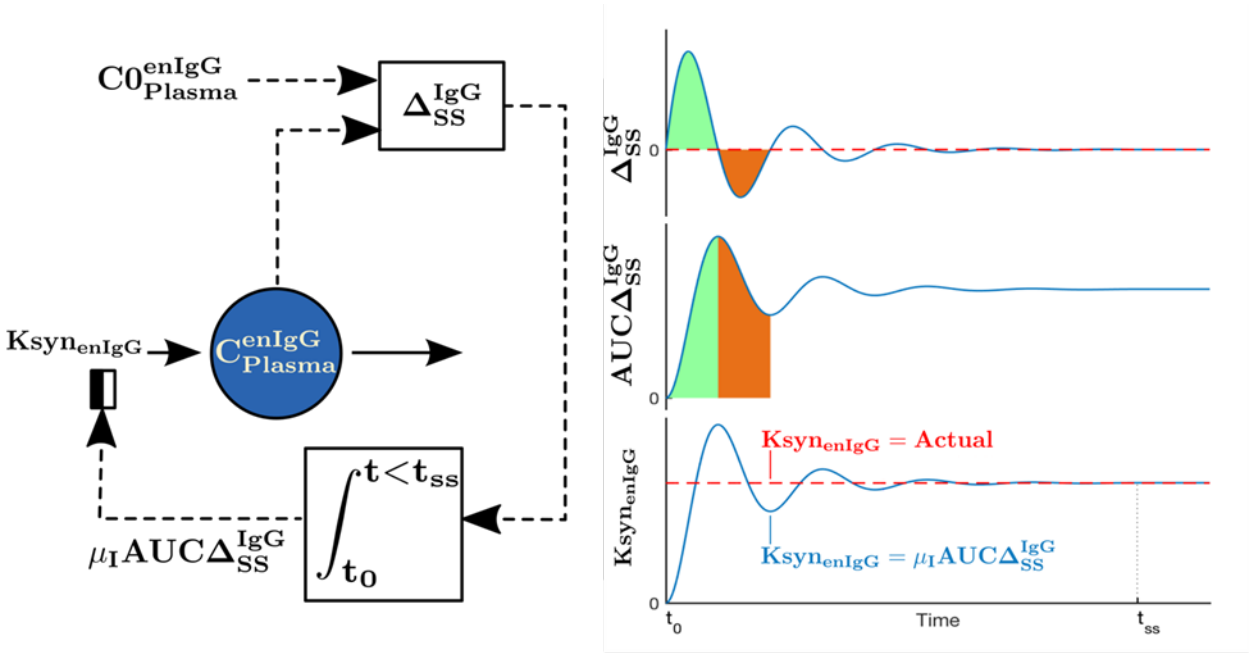

Supplementary Figure 1. Determination of steady state synthesis of an endogenous species (IgG) using an integral controller.

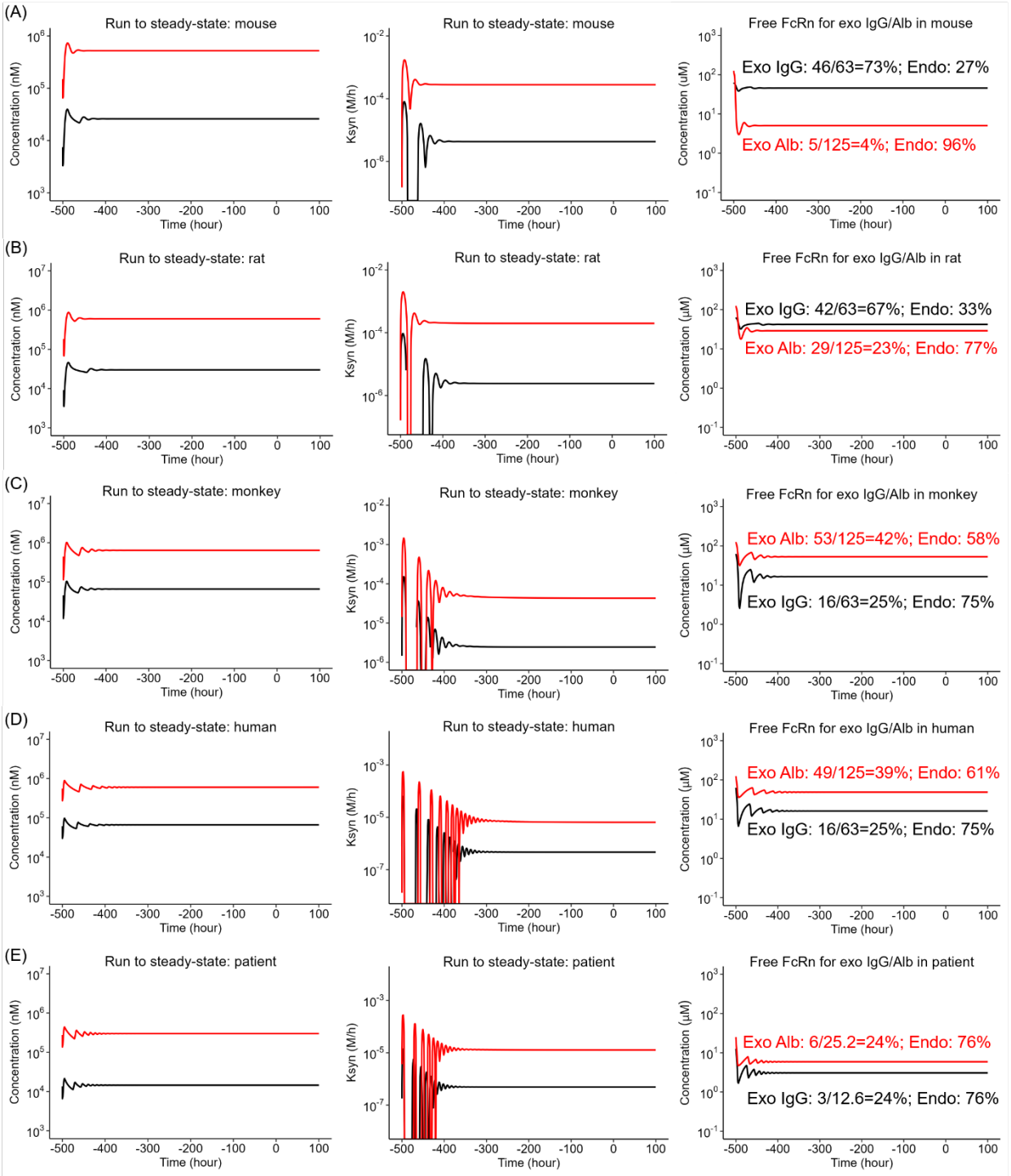

Supplementary Figure 2. Time courses of plasma concentrations of endogenous IgG and albumin (left column), synthesis rates of endogenous IgG and albumin (middle column), and

endosomal free FcRn concentrations (in liver as an example) available for exogenous IgG and albumin binding (right column), in (A) mice, (B) rats, (C) monkeys, (D) healthy humans, and (E) FHH patients during the PBPK model stabilization period. Curves associated with IgG and albumin are colored black and red, respectively. The fractions of total FcRn occupied by endogenous IgG/albumin and available for exogenous IgG/albumin binding are also provided.

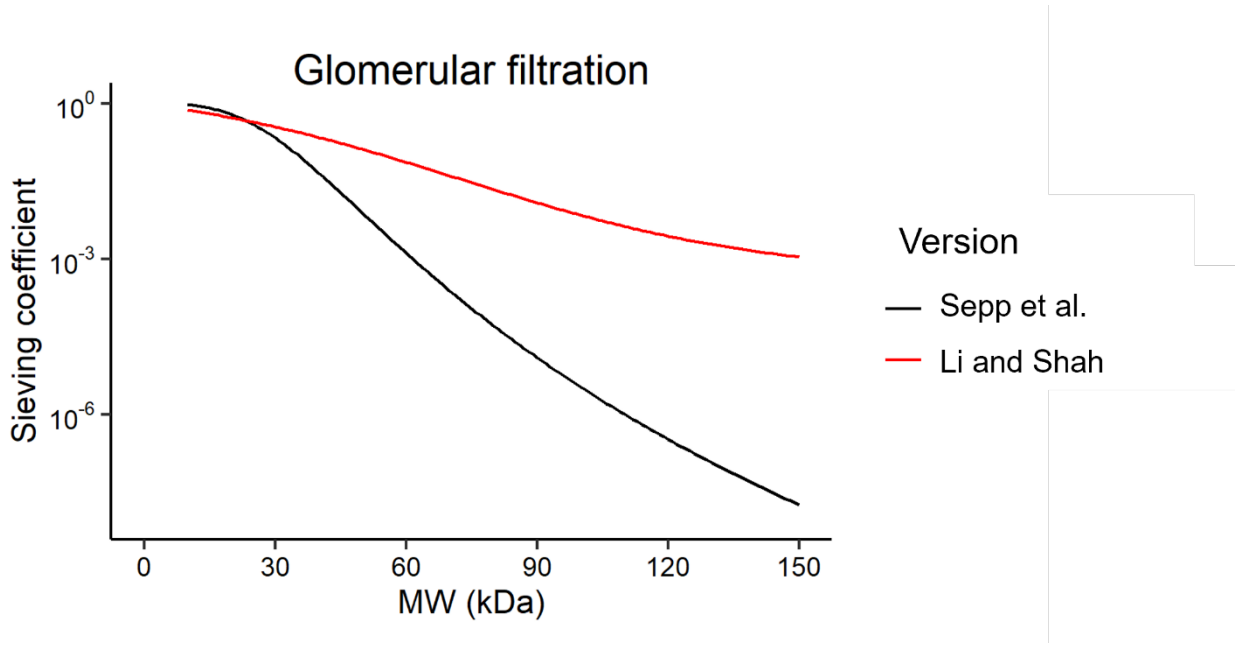

Supplementary Figure 3. Distinct molecular size-dependent renal sieving coefficients described by equations taken from Sepp et al. [2] and Li and Shah [3].

Pathway analysis

To understand the importance of different mechanisms in eliminating different-size proteins in humans, contribution of renal filtration and lysosomal degradation was simulated:

$$\%\ Renal\ filtration = \frac{\int\left(GFR\cdot\theta_{SUB}\cdot C_{Kidney}^{V,SUB}\right)dt}{\int\left(GFR\cdot\theta_{SUB}\cdot C_{Kidney}^{V,SUB}\right)dt+\sum_{i=All\ organs}\int\left(K_{deg}\cdot C_i^{E,UB,SUB}\cdot V_i^E\right)dt}\times 100\% \quad (5)$$

$$\%\ Lysosomal\ catabolism = \frac{\sum_{i=All\ organs}\int\left(K_{deg}\cdot C_i^{E,UB,SUB}\cdot V_i^E\right)dt}{\int\left(GFR\cdot\theta_{SUB}\cdot C_{Kidney}^{V,SUB}\right)dt+\sum_{i=All\ organs}\int\left(K_{deg}\cdot C_i^{E,UB,SUB}\cdot V_i^E\right)dt}\times 100\% \quad (6)$$

Note that this approach applies to molecules without FcRn binding or with the IgG1 Fc, without albumin binding, and without tubular reabsorption.

The following equations were used to calculate transcapillary mass transport of different-size proteins attributed to diffusive/convective transport through large and small pores and transcytosis in humans:

$$Mass_{L,diffusion} = \sum_{i=All\ organs}\int\left(PS_{L,i}^{SUB}\cdot\left(C_i^{V,SUB}-C_i^{I,SUB}\right)\cdot\frac{Pe_{L,i}^{SUB}}{e^{Pe_{L,i}^{SUB}}-1}\right)dt \quad (7)$$

$$Mass_{S,diffusion} = \sum_{i=All\ organs}\int\left(PS_{S,i}^{SUB}\cdot\left(C_i^{V,SUB}-C_i^{I,SUB}\right)\cdot\frac{Pe_{S,i}^{SUB}}{e^{Pe_{S,i}^{SUB}}-1}\right)dt \quad (8)$$

$$Mass_{L,convection} = \sum_{i=All\ organs}\int J_{L,i}\cdot\left(1-\sigma_L^{SUB}\right)\cdot C_i^{V,SUB}dt \quad (9)$$

$$Mass_{S,convection} = \sum_{i=All\ organs}\int J_{S,i}\cdot\left(1-\sigma_S^{SUB}\right)\cdot C_i^{V,SUB}dt \quad (10)$$

$$Mass_{transcytosis} = \sum_{i=All\ organs}\int 2\ CL_{up}^i\cdot(1-FR)\cdot C_i^{E,B,SUB}\cdot\frac{CL_{up}^i\cdot C_i^{V,SUB}}{CL_{up}^i\cdot\left(C_i^{V,SUB}+C_i^{I,SUB}\right)}\ dt \quad (11)$$

$$\%\ Large\ pore\ diffusion = \quad (12)$$

$$\frac{Mass_{L,diffusion}}{Mass_{L,diffusion}+Mass_{S,diffusion}+Mass_{L,convection}+Mass_{S,convection}+Mass_{transcytosis}}\times 100\%$$

$$\%\ Small\ pore\ diffusion = \quad (13)$$

$$\frac{Mass_{S,diffusion}}{Mass_{L,diffusion}+Mass_{S,diffusion}+Mass_{L,convection}+Mass_{S,convection}+Mass_{transcytosis}}\times 100\%$$

$$\%\ Large\ pore\ convection = \frac{Mass_{L,convection}}{Mass_{L,diffusion}+Mass_{S,diffusion}+Mass_{L,convection}+Mass_{S,convection}+Mass_{transcytosis}} \times 100\% \quad (14)$$

$$\%\ Small\ pore\ convection = \frac{Mass_{S,convection}}{Mass_{L,diffusion}+Mass_{S,diffusion}+Mass_{L,convection}+Mass_{S,convection}+Mass_{transcytosis}} \times 100\% \quad (15)$$

$$\%\ Transcytosis = \frac{Mass_{transcytosis}}{Mass_{L,diffusion}+Mass_{S,diffusion}+Mass_{L,convection}+Mass_{S,convection}+Mass_{transcytosis}} \times 100\% \quad (16)$$

In all these simulations, the duration was set to 10000 hours, by which time most of the protein molecules are considered to have been eliminated from the system. In simulations involving FcRn binding, the lower bound of the MW range investigated is 50 kDa, roughly corresponding to the size of Fc.

Supplementary Table 1. Study details and respective model variants of modalities incorporated in the two-pore PBPK development.

Species	Modality	MW (kDa)	Dose level	Model variant [a]	Reference	PK linearity category [c]
Mouse	scFv-IgAb	205	10 mg/kg	$MW_{exoIgG} = 2.05 \times 10^5$	[4]	1
	Human IgG1	150	0.3 and 5 mg/kg	-	[5]	2
	Human IgG1	150	10 mg/kg	-	[6]	1
	FcRn-nonbinding human IgG1	150	10 mg/kg	$K_{on}^{FcRn,exoIgG} = 0$	[6]	1
	Human IgG1 in FcRn KO	150	5 mg/kg		[7]	3
	Murine IgG1 in FcRn KO	150	8 mg/kg		[8]	1
	TandAb	110	10 mg/kg	$K_{on}^{FcRn,exoIgG} = 0$, $MW_{exoIgG} = 1.1 \times 10^5$	[4]	1
	scFv-Fc	105	2-5 µg/animal	$MW_{exoIgG} = 1.05 \times 10^5$	[9]	3
	F(ab)2	100	10 mg/kg	$K_{on}^{FcRn,exoIgG} = 0$, $MW_{exoIgG} = 1 \times 10^5$	[6]	1
	F(ab)2	100	5 µg/animal		[10]	4
	Minibody	80	0.125 µg/animal	$K_{on}^{FcRn,exoIgG} = 0$, $MW_{exoIgG} = 8 \times 10^4$	[11]	4
	Mouse albumin	67	2.5 mg/kg	-	[2]	1
	Nanobody-PAS600	60	10 mg/kg	$K_{on}^{FcRn,exoIgG} = 0$, $MW_{exoIgG} = 6 \times 10^4$	[12]	2
	Fab	50	10 mg/kg	$K_{on}^{FcRn,exoIgG} = 0$, $MW_{exoIgG} = 5 \times 10^4$	[6]	1
	Fab	50	12 µg/animal		[13]	4
	Fab	50	25 µg/animal		[14]	4
	Fab	50	4 µg/animal		[15]	4
	Diabody	50	20 µg/animal	$K_{on}^{FcRn,exoIgG} = 0$, $MW_{exoIgG} = 5 \times 10^4$	[16]	4
	scFv	27	10 mg/kg	$K_{on}^{FcRn,exoIgG} = 0$,	[6]	1

	scFv	27	1.67 μg/animal	$MW_{exoIgG} = 2.7 \times 10^4$	[17]	4
	scFv	27	0.4 μg/animal		[18]	4
	scFv	27	100 μg/animal		[19]	4
	Albud (dAb2)	23.5	10 mg/kg	$K_{on}^{Alb,Albud} = 7.7 \times 10^8$, $K_{off}^{Alb,Albud} = 100$, $MW_{Albud} = 2.35 \times 10^4$, $MW_{AlbudAl} = 9.05 \times 10^4$	[2]	1
	dAb2	23.5	10 mg/kg	$K_{on}^{FcRn,exoIgG} = 0$, $MW_{exoIgG} = 2.35 \times 10^4$	[2]	1
	Nanobody	13	10 mg/kg	$K_{on}^{FcRn,exoIgG} = 0$, $MW_{exoIgG} = 1.3 \times 10^4$	[6]	1
Rat	Human IgG1	150	2.5 mg/kg	-	[2]	1
	Human IgG1	150	10 mg/kg	-	[20]	1
	FcRn-nonbinding human IgG1	150	10 mg/kg	$K_{on}^{FcRn,exoIgG} = 0$	[20]	1
	F(ab)2	100	10 mg/kg	$K_{on}^{FcRn,exoIgG} = 0$, $MW_{exoIgG} = 1 \times 10^5$	[20]	1
	F(ab)2	100	0.7 mg/kg		[21]	1
	Fc-fusion	92	10 mg/kg	$MW_{exoIgG} = 9.2 \times 10^4$	[22]	2
	Rat albumin	67	2.5 mg/kg	-	[2]	1
	Fc-fusion	60	0.3 mg/kg	$MW_{exoIgG} = 6 \times 10^4$	[23]	2
	Nanobody-PAS600	60	3.5 mg/kg	$K_{on}^{FcRn,exoIgG} = 0$, $MW_{exoIgG} = 6 \times 10^4$	[12]	3
	Fab	50	10 mg/kg	$K_{on}^{FcRn,exoIgG} = 0$, $MW_{exoIgG} = 5 \times 10^4$	[20]	1
	Fab	50	0.7 mg/kg		[21]	1
	Fab	50	1 mg/kg		[24]	2
	scFv	27	10 mg/kg	$K_{on}^{FcRn,exoIgG} = 0$, $MW_{exoIgG} = 2.7 \times 10^4$	[20]	1
	dAb2	23.5	10 mg/kg	$K_{on}^{FcRn,exoIgG} = 0$,	[2]	1

				$MW_{exoIgG} = 2.35 \times 10^4$		
	Inulin	5.5	20 mg/kg	$K_{on}^{FcRn,exoIgG} = 0$, $MW_{exoIgG} = 5.5 \times 10^3$	[25]	1
Monkey	scFv-IgAb	205	5 mg/kg	$MW_{exoIgG} = 2.05 \times 10^5$	[26]	1
	DVD-Ig	200	5 mg/kg	$MW_{exoIgG} = 2 \times 10^5$	[27]	3
	Human IgG1	150	1 mg/kg	-	[28]	4
	Human IgG1	150	30 mg/kg	-	[29]	3
	Human IgG1	150	5 mg/kg	-	[30]	3
	Human IgG1	150	20 mg/kg	-	[31]	2
	Human IgG1	150	3 mg/kg	-	[32]	2
	scFv-Fc	110	1.5 mg/kg	$MW_{exoIgG} = 1.1 \times 10^5$	[33]	2
	scFv-Fc	110	60 ug/kg		[34]	2
	F(ab)2	100	5 mg/kg	$K_{on}^{FcRn,exoIgG} = 0$, $MW_{exoIgG} = 1 \times 10^5$	[35]	2
	IFNα-human albumin conjugate	85.7	30 μg/kg	$K_{on}^{FcRn,exoAlb} = 1.9 \times 10^7$, $K_{off}^{FcRn,exoAlb} = 46.8$, $MW_{exoAlb} = 8.57 \times 10^4$	[36]	2
	Nanobody-PAS600	60	2 mg/kg	$K_{on}^{FcRn,exoIgG} = 0$, $MW_{exoIgG} = 6 \times 10^4$	[12]	2
	Fab	50	1 and 4 mg/animal	$K_{on}^{FcRn,exoIgG} = 0$, $MW_{exoIgG} = 5 \times 10^4$	[37]	2
	Fab	50	5 mg/kg		[38]	1
	Nanobody-Albud	26	2 mg/kg	$K_{on}^{Alb,Albud} = 1 \times 10^9$, $K_{off}^{Alb,Albud} = 31$, $MW_{Albud} = 2.6 \times 10^4$, $MW_{AlbudAl} = 9.3 \times 10^4$	[39]	1
	Anticalin-Albud	22	3 mg/kg	$K_{on}^{Alb,Albud} = 1 \times 10^9$, $K_{off}^{Alb,Albud} = 0.019$,	[40]	2

				$MW_{Albud} = 2.2 \times 10^4$, $MW_{AlbudAl} = 8.9 \times 10^4$		
	dAb-Albud	16	3 mg/kg	$K_{on}^{Alb,Albud} = 4.068 \times 10^9$, $K_{off}^{Alb,Albud} = 0.244$, $MW_{Albud} = 1.6 \times 10^4$, $MW_{AlbudAl} = 8.3 \times 10^4$	[41]	1
	Albud (DARPin)	14	0.75 mg/kg	$K_{on}^{Alb,Albud} = 1 \times 10^9$, $K_{off}^{Alb,Albud} = 0.019$, $MW_{Albud} = 1.4 \times 10^4$, $MW_{AlbudAl} = 8.1 \times 10^4$	[42]	1
	Nanobody	13	2 mg/kg	$K_{on}^{FcRn,exoIgG} = 0$, $MW_{exoIgG} = 1.3 \times 10^4$	[39]	1
Human	Human IgG1	150	5 mg/kg	-	[43]	1
	Human IgG1	150	1 mg/subject	-	[44]	4
	Human IgG1 in FHH patients	150	25 μCi/subject	$FcRn\_0^{IgG} = 1.25 \times 10^{-5}$ [b] $C\_0_{Plasma}^{enIgG} = 1.452 \times 10^{-5}$ $C\_0_{Plasma}^{enAlb} = 2.985 \times 10^{-4}$	[45]	1
	F(ab)2	100	2 mg/kg	$K_{on}^{FcRn,exoIgG} = 0$, $MW_{exoIgG} = 1 \times 10^5$	[46]	2
	Fc-fusion	92	20 mg/kg	$MW_{exoIgG} = 9.2 \times 10^4$	[47]	2
	Fc-fusion	84	20 mg/kg	$MW_{exoIgG} = 8.4 \times 10^4$	[48]	2
	Fc-fusion	80.5	10 mg/kg	$MW_{exoIgG} = 8.05 \times 10^4$	[48]	2
	Albumin	67	30-60 mg/subject	-	[49]	1
	Fc-fusion	65	30 mg/kg	$MW_{exoIgG} = 6.5 \times 10^4$	[50]	2
	scFv-PE	65	20 μg/kg	$K_{on}^{FcRn,exoIgG} = 0$, $MW_{exoIgG} = 6.5 \times 10^4$	[51]	2
	Fab	50	5 g/subject	$K_{on}^{FcRn,exoIgG} = 0$, $MW_{exoIgG} = 5 \times 10^4$	[52]	3
	Fab	50	8 g/subject		[53]	2

	Fab	50	0.25 mg/kg		[54]	4
	Fab	50	4 mg/subject		[55]	2
	dAb-Albud	13	1 mg/subject	$K_{on}^{Alb,Albud} = 3.6 \times 10^9$, $K_{off}^{Alb,Albud} = 3.1$, $MW_{Albud} = 1.3 \times 10^4$, $MW_{AlbudAl} = 8 \times 10^4$	[56]	1

[a] A model variant contains parameter values and/or initial conditions that are different from default values defined in the manuscript. Molecules with no FcRn interactions are represented as "$exoIgG$". Albumin conjugates are represented as "$exoAlb$". Albud proteins are represented as "$Albud$".

[b] The endosomal total FcRn concentration in FHH patients is assumed to be 20% of that in healthy humans based on an *in vitro* gene expression study [57].

[c] Digitized data belong to 1 of the 4 categories of PK linearity determination. Category 1: There is no target-binding in the species investigated. Category 2: Multiple dose levels have been tested/reported and PK linearity was verified. Category 3: The dose level was considered sufficiently high to saturate potential target binding. Category 4: When the dose level was not obviously high to saturate target binding, linear PK was assumed with caution if the data were consistent with other linear PK data for proteins with a similar MW, or if the data was used in previous publications for linear PBPK model validation.

References

1. Abuqayyas, L. and J. Harrold. *A General Method for Initialization of Steady-States in Complex PK/PD Systems*. in *JOURNAL OF PHARMACOKINETICS AND PHARMACODYNAMICS*. 2015. SPRINGER/PLENUM PUBLISHERS 233 SPRING ST, NEW YORK, NY 10013 USA.
2. Sepp, A., et al., *Computer-assembled cross-species/cross-modalities two-pore physiologically based pharmacokinetic model for biologics in mice and rats.* J Pharmacokinet Pharmacodyn, 2019. **46**(4): p. 339-359.
3. Li, Z. and D.K. Shah, *Two-pore physiologically based pharmacokinetic model with de novo derived parameters for predicting plasma PK of different size protein therapeutics.* J Pharmacokinet Pharmacodyn, 2019. **46**(3): p. 305-318.
4. Ellwanger, K., et al., *Redirected optimized cell killing (ROCK(R)): A highly versatile multispecific fit-for-purpose antibody platform for engaging innate immunity.* MAbs, 2019. **11**(5): p. 899-918.
5. Yeung, Y.A., et al., *A therapeutic anti-VEGF antibody with increased potency independent of pharmacokinetic half-life.* Cancer Res, 2010. **70**(8): p. 3269-77.
6. Li, Z., et al., *Two-pore physiologically based pharmacokinetic model validation using whole-body biodistribution of trastuzumab and different-size fragments in mice.* J Pharmacokinet Pharmacodyn, 2021. **48**(5): p. 743-762.
7. Avery, L.B., et al., *Utility of a human FcRn transgenic mouse model in drug discovery for early assessment and prediction of human pharmacokinetics of monoclonal antibodies.* MAbs, 2016. **8**(6): p. 1064-78.
8. Garg, A. and J.P. Balthasar, *Physiologically-based pharmacokinetic (PBPK) model to predict IgG tissue kinetics in wild-type and FcRn-knockout mice.* J Pharmacokinet Pharmacodyn, 2007. **34**(5): p. 687-709.
9. Olafsen, T., V.E. Kenanova, and A.M. Wu, *Tunable pharmacokinetics: modifying the in vivo half-life of antibodies by directed mutagenesis of the Fc fragment.* Nat Protoc, 2006. **1**(4): p. 2048-60.
10. Pedley, R.B., et al., *Comparative radioimmunotherapy using intact or F(ab')2 fragments of 131I anti-CEA antibody in a colonic xenograft model.* Br J Cancer, 1993. **68**(1): p. 69-73.
11. Hu, S., et al., *Minibody: A novel engineered anti-carcinoembryonic antigen antibody fragment (single-chain Fv-CH3) which exhibits rapid, high-level targeting of xenografts.* Cancer Res, 1996. **56**(13): p. 3055-61.
12. Griffiths, K., et al., *Half-life extension and non-human primate pharmacokinetic safety studies of i-body AD-114 targeting human CXCR4.* MAbs, 2019. **11**(7): p. 1331-1340.
13. Burak, W.E., Jr., et al., *Biodistribution and localization of radiolabeled NR-LU-10 Fab fragment in human breast cancer xenografts.* Nucl Med Biol, 1998. **25**(7): p. 633-7.
14. Hadley, S.W., et al., *Astatine-211 labeling of an antimelanoma antibody and its Fab fragment using N-succinimidyl p-astatobenzoate: comparisons in vivo with the p-[125I]iodobenzoyl conjugate.* Bioconjug Chem, 1991. **2**(3): p. 171-9.
15. Kamigaki, T., et al., *Therapy and imaging of pancreatic carcinoma xenografts with radioiodine-labeled chimeric monoclonal antibody A10 and its Fab fragment.* Jpn J Cancer Res, 1995. **86**(12): p. 1216-23.
16. Adams, G.P., et al., *Prolonged in vivo tumour retention of a human diabody targeting the extracellular domain of human HER2/neu.* Br J Cancer, 1998. **77**(9): p. 1405-12.
17. Pavlinkova, G., et al., *Pharmacokinetics and biodistribution of engineered single-chain antibody constructs of MAb CC49 in colon carcinoma xenografts.* J Nucl Med, 1999. **40**(9): p. 1536-46.
18. Wu, A.M., et al., *Tumor localization of anti-CEA single-chain Fvs: improved targeting by non-covalent dimers.* Immunotechnology, 1996. **2**(1): p. 21-36.

19. Adams, G.P., et al., *Highly specific in vivo tumor targeting by monovalent and divalent forms of 741F8 anti-c-erbB-2 single-chain Fv.* Cancer Res, 1993. **53**(17): p. 4026-34.
20. Chang, H.Y., et al., *Effect of the Size of Protein Therapeutics on Brain Pharmacokinetics Following Systematic Administration.* AAPS J, 2022. **24**(3): p. 62.
21. Bazin-Redureau, M.I., C.B. Renard, and J.M. Scherrmann, *Pharmacokinetics of heterologous and homologous immunoglobulin G, F(ab')2 and Fab after intravenous administration in the rat.* J Pharm Pharmacol, 1997. **49**(3): p. 277-81.
22. Lon, H.K., et al., *Modeling pharmacokinetics/pharmacodynamics of abatacept and disease progression in collagen-induced arthritic rats: a population approach.* J Pharmacokinet Pharmacodyn, 2013. **40**(6): p. 701-12.
23. Wang, Y.M., et al., *Investigation of the pharmacokinetics of romiplostim in rodents with a focus on the clearance mechanism.* Pharm Res, 2011. **28**(8): p. 1931-8.
24. Kularatne, S.A., et al., *Recruiting cytotoxic T cells to folate-receptor-positive cancer cells.* Angew Chem Int Ed Engl, 2013. **52**(46): p. 12101-12104.
25. Tsuji, A., et al., *Physiologically based pharmacokinetic model for beta-lactam antibiotics I: Tissue distribution and elimination in rats.* J Pharm Sci, 1983. **72**(11): p. 1239-52.
26. Datta-Mannan, A., et al., *Pharmacokinetic Developability and Disposition Profiles of Bispecific Antibodies: A Case Study with Two Molecules.* Antibodies (Basel), 2021. **11**(1).
27. Tarcsa, E., et al., *Dual-variable domain immunoglobulin (DVD-Ig™) technology: a versatile, novel format for the next generation of dual-targeting biologics.* Bispecific antibodies, 2011: p. 171-185.
28. Haunschild, J., et al., *Pharmacokinetics of reshaped MAb 425 in three animal species.* Cell Biophys, 1995. **26**(3): p. 167-82.
29. Dall'Acqua, W.F., P.A. Kiener, and H. Wu, *Properties of human IgG1s engineered for enhanced binding to the neonatal Fc receptor (FcRn).* J Biol Chem, 2006. **281**(33): p. 23514-24.
30. Aweda, T.A., et al., *In vivo biodistribution and pharmacokinetics of sotrovimab, a SARS-CoV-2 monoclonal antibody, in healthy cynomolgus monkeys.* Eur J Nucl Med Mol Imaging, 2023. **50**(3): p. 667-678.
31. Vugts, D.J., et al., *Preclinical evaluation of 89Zr-labeled anti-CD44 monoclonal antibody RG7356 in mice and cynomolgus monkeys: Prelude to Phase 1 clinical studies.* MAbs, 2014. **6**(2): p. 567-75.
32. Cole, E.L., et al., *Radiosynthesis and preclinical PET evaluation of (89)Zr-nivolumab (BMS-936558) in healthy non-human primates.* Bioorg Med Chem, 2017. **25**(20): p. 5407-5414.
33. Smith, R.A., et al., *ASN004, A 5T4-targeting scFv-Fc Antibody-Drug Conjugate with High Drug-to-Antibody Ratio, Induces Complete and Durable Tumor Regressions in Preclinical Models.* Mol Cancer Ther, 2021. **20**(8): p. 1327-1337.
34. Root, A.R., et al., *Discovery and optimization of a novel anti-GUCY2c x CD3 bispecific antibody for the treatment of solid tumors.* MAbs, 2021. **13**(1): p. 1850395.
35. Couch, J.A., et al., *Balancing Efficacy and Safety of an Anti-DLL4 Antibody through Pharmacokinetic Modulation.* Clin Cancer Res, 2016. **22**(6): p. 1469-79.
36. Osborn, B.L., et al., *Pharmacokinetic and pharmacodynamic studies of a human serum albumin-interferon-alpha fusion protein in cynomolgus monkeys.* J Pharmacol Exp Ther, 2002. **303**(2): p. 540-8.
37. Gaudreault, J., et al., *Preclinical pharmacokinetics of Ranibizumab (rhuFabV2) after a single intravitreal administration.* Invest Ophthalmol Vis Sci, 2005. **46**(2): p. 726-33.
38. Datta-Mannan, A., et al., *Engineered FcRn Binding Fusion Peptides Significantly Enhance the Half-Life of a Fab Domain in Cynomolgus Monkeys.* Biotechnol J, 2019. **14**(3): p. e1800007.

39. Hoefman, S., et al., *Pre-clinical intravenous serum pharmacokinetics of albumin binding and non-half-life extended Nanobodies®.* Antibodies, 2015. **4**(3): p. 141-156.
40. Masuda, Y., et al., *Generation and Characterization of a Novel Small Biologic Alternative to Proprotein Convertase Subtilisin/Kexin Type 9 (PCSK9) Antibodies, DS-9001a, Albumin Binding Domain-Fused Anticalin Protein.* J Pharmacol Exp Ther, 2018. **365**(2): p. 368-378.
41. Jacobs, S.A., et al., *Fusion to a highly stable consensus albumin binding domain allows for tunable pharmacokinetics.* Protein Eng Des Sel, 2015. **28**(10): p. 385-93.
42. Steiner, D., et al., *Half-life extension using serum albumin-binding DARPin(R) domains.* Protein Eng Des Sel, 2017. **30**(9): p. 583-591.
43. Shah, D.K. and A.M. Betts, *Towards a platform PBPK model to characterize the plasma and tissue disposition of monoclonal antibodies in preclinical species and human.* J Pharmacokinet Pharmacodyn, 2012. **39**(1): p. 67-86.
44. Buist, M.R., et al., *Kinetics and tissue distribution of the radiolabeled chimeric monoclonal antibody MOv18 IgG and F(ab')2 fragments in ovarian carcinoma patients.* Cancer Res, 1993. **53**(22): p. 5413-8.
45. Waldmann, T.A. and W.D. Terry, *Familial hypercatabolic hypoproteinemia. A disorder of endogenous catabolism of albumin and immunoglobulin.* J Clin Invest, 1990. **86**(6): p. 2093-8.
46. Allison, D.E., et al., *Pharmacokinetics of rhuMAb CD18, a recombinant humanised monoclonal antibody fragment to CD18, in normal healthy human volunteers.* BioDrugs, 2002. **16**(1): p. 63-70.
47. Ma, Y., et al., *Pharmacokinetics of CTLA4Ig fusion protein in healthy volunteers and patients with rheumatoid arthritis.* Acta Pharmacol Sin, 2009. **30**(3): p. 364-71.
48. Yang, J., et al., *First-in-human study of the safety, tolerability, pharmacokinetics, and pharmacodynamics of ALPN-101, a dual CD28/ICOS antagonist, in healthy adult subjects.* Clin Transl Sci, 2021. **14**(4): p. 1314-1326.
49. Beeken, W.L., et al., *Studies of I-131-albumin catabolism and distribution in normal young male adults.* J Clin Invest, 1962. **41**: p. 1312-33.
50. Herbst, R.S., et al., *Safety, pharmacokinetics, and antitumor activity of AMG 386, a selective angiopoietin inhibitor, in adult patients with advanced solid tumors.* J Clin Oncol, 2009. **27**(21): p. 3557-65.
51. von Minckwitz, G., et al., *Phase I clinical study of the recombinant antibody toxin scFv(FRP5)-ETA specific for the ErbB2/HER2 receptor in patients with advanced solid malignomas.* Breast Cancer Res, 2005. **7**(5): p. R617-26.
52. Glund, S., et al., *Effect of Age and Renal Function on Idarucizumab Pharmacokinetics and Idarucizumab-Mediated Reversal of Dabigatran Anticoagulant Activity in a Randomized, Double-Blind, Crossover Phase Ib Study.* Clin Pharmacokinet, 2017. **56**(1): p. 41-54.
53. Yasaka, M., et al., *Safety, pharmacokinetics and pharmacodynamics of idarucizumab, a specific dabigatran reversal agent in healthy Japanese volunteers: a randomized study.* Res Pract Thromb Haemost, 2017. **1**(2): p. 202-215.
54. Mager, D.E., et al., *Simultaneous modeling of abciximab plasma concentrations and ex vivo pharmacodynamics in patients undergoing coronary angioplasty.* J Pharmacol Exp Ther, 2003. **307**(3): p. 969-76.
55. Macfarlane, D.J., et al., *Safety, pharmacokinetic and dosimetry evaluation of the proposed thrombus imaging agent 99mTc-DI-DD-3B6/22-80B3 Fab'.* Eur J Nucl Med Mol Imaging, 2006. **33**(6): p. 648-56.
56. Sepp, A., M. Bergstrom, and M. Davies, *Cross-species/cross-modality physiologically based pharmacokinetics for biologics: 89Zr-labelled albumin-binding domain antibody GSK3128349 in humans.* MAbs, 2020. **12**(1): p. 1832861.

57. Wani, M.A., et al., *Familial hypercatabolic hypoproteinemia caused by deficiency of the neonatal Fc receptor, FcRn, due to a mutant beta2-microglobulin gene.* Proc Natl Acad Sci U S A, 2006. **103**(13): p. 5084-9.